Low-Cost and High-Performance Electrospun Carbon Nanofiber Film Anodes

Jianxin Cai[1], Wei Li[1], Pengfei Zhao[1], Ji Yu[2], Zhenyu Yang[2,]*

[1] School of Resources Environmental and Chemical Engineering, Nanchang University, No. 999 Xuefu Road, Nanchang, Jiangxi,330031, P. R. China
[2] School of Chemistry, Nanchang University, No.999 Xuefu Road, Nanchang, Jiangxi, 330031, P. R. China
[*]E-mail: cjx@ncu.edu.cn

Carbon nanofiber thin membrane is a promising candidate material for chemical power supply because of its simple design and fast charge-transfer network. In this study, the original porous carbon nanofiber thin membrane electrode was electrospun following a simple and rapid washing process. The structural features of the porous carbon nanofiber membranes were characterized by scanning electron microscopy, transmission electron microscopy, X-ray diffraction, and Brunauer–Emmett–Teller analysis. The electrochemical performance of the porous carbon nanofiber membranes was investigated by electrochemical test. Results show that the as-prepared porous carbon nanofiber film possesses a highly porous surface structure and demonstrates an outstanding electrochemical performance. The film electrode exhibits a charge capacity of 948.1 mAh·g^{-1} under a C-rate of 0.1C (37.2 mA·g^{-1}) and 208.8 mAh·g^{-1} after 1700 cycles under a C-rate of 5C (1860 mA·g^{-1}). In the preparation of a binder- and conductive-free thin film electrode, the addition of NaCl increases the precursor viscosity, which results in a slimmer fiber and significantly improves the specific surface area by washing NaCl crystals with water. This method avoids rinsing with an acidic or basic solution and recycles the used NaCl, thereby significantly reducing the preparation cost of porous carbon fiber thin film electrode. This work demonstrates a new method of preparing high-value porous carbon fiber thin film electrodes at a low cost.

1. INTRODUCTION

Given the increasing demand for electronic equipment, the development of high-efficiency and high-capacity storage systems has attracted considerable attention. An electrode is a crucial element that affects the performance of energy-storage devices. Carbon-based electrode materials are widely

used in various energy-storage devices owing to their light weight, high stability, high conductivity, and low cost [1–4]. Among a variety of energy storage systems, high-performance lithium-ion batteries (LIBs) are believed to be a valid solution to the increasing demand for high energy-density electronic equipment [5–11]. At present, the rechargeable LIB anode material is mainly composed of graphite [12]. Unfortunately, the energy density and power capability of graphite are unsuitable for new-generation LIBs [13, 14]. To address these shortcomings, researchers have applied nanotechnology to improve carbon materials such as graphene nanosheets, aligned carbon nanotubes, activated carbon, and carbon aerogels as anodes for LIBs [15–17]. These nanostructured carbon materials used in LIBs exhibit electrochemical properties superior to those of graphite. However, nanotechnological processes are unsuitable for mass production because of the typically complex, cost-ineffective, and harsh synthesis conditions of the additional chemical treatments required during the nanotechnological processes [18–21].

Electrospinning is a simple, efficient, economical technique for the large-scale fabrication of concatenated nanofibers [22]. This technique is often used in the development of nanostructures consisting of ceramics, metals, carbon, or their composites. Recently, carbon nanofibers prepared using electrospinning and subsequent carbonization have been utilized as high-performance anodes for LIBs owing to the improved electron transfer capabilities imparted by their web-like structures [23–25]. Electrospinning can also be coupled with other simple treatments (pyrolysis or etching with gas) to produce porous carbon nanofiber materials [26–28]. Porous carbon nanofibers have a linear, continuous, interconnected network structure when used as an anode for LIBs. The special structure of porous carbon nanofibers not only increases the lithium ion storage sites and electron conduction pathways but also reduces the distance of lithium ion diffusion, thus reducing the resistance and increasing the capacity of LIBs.

In this report, a simple and low-cost method to prepare porous carbon nanofibers by electrospinning polyvinylpyrrolidone (PVP)/sodium chloride (NaCl), followed by carbonization, and rinsing with deionized water is employed. In the preparation of a binder- and conductive-free thin film electrode, the addition of NaCl increases the precursor viscosity, which results in a slimmer fiber and significantly improves the specific surface area by washing NaCl crystals with water. This method avoids rinsing with an acidic or basic solution and recycles the used NaCl, thereby significantly reducing the preparation cost of porous carbon fiber thin film electrodes. The resultant porous carbon nanofiber film with a highly porous surface structure can be directly used as an anode for LIBs without binder and conductive addition agents, and the thin film electrodes display outstanding electrochemical performance.

2. EXPERIMENTAL

2.1 Preparation of porous carbon nanofibers

PVP (Mw=1,300,000), NaCl, and anhydrous ethanol were obtained from Sinopharm Chemical Reagent Co., Ltd., and water was prepared in the laboratory. All chemical reagents were used directly. A porous carbon nanofiber thin film was prepared by electrospinning combined with annealing. In the

experiment, 1.17 g of NaCl was dissolved in 12 mL of deionized water, which was sequentially added with 12 mL of absolute ethanol and 2.34 g of PVP with magnetic stirring for 24 h. The PVP concentration to the whole solution is approximately 10 wt%. Then, the solution was electrospun under 20 kV direct-current voltage at a flow rate of 0.2 mL·h^{-1}. The distance from the roller to the needle was 20 cm.

The PVP/NaCl polymer nanofiber thin film was first stabilized in air at 280 °C for 2 h at a heating rate of 5 °C/min and carbonized in Ar atmosphere at 600 °C for 2 h at a heating rate of 2 °C/min, producing C/NaCl nanofiber thin film. Finally, the C/NaCl nanofiber thin film was soaked in deionized water for 30 min, removed from the deionized water, and then rinsed repeatedly until no Cl^{-1} was detected in the eluent, thereby generating a porous carbon nanofiber thin film. Using the same treatment, we obtained the carbon nanofiber thin film by electrospinning PVP.

2.2 Characterization

The morphology and diameter of PVP/NaCl nanofibers, C/NaCl nanofibers, and porous carbon nanofibers were evaluated using scanning electron microscopy (SEM, Philips-FEI, Tecnai Quanta200F), and the structure and distribution of pores in the porous carbon nanofibers were characterized by transmission electron microscopy (TEM, Tecnai G2 F20) and Brunauer–Emmett–Teller (BET) analysis. The crystalline structure of the carbonized specimens was identified using X-ray diffraction (XRD) by a diffractometer (Bruker D8 Focus) with a 2θ range from 5° to 80°.

2.3 Electrochemical performance evaluation

The electrochemical performance of the porous carbon nanofiber thin film was evaluated using a 2025-type cell, and the porous carbon nanofiber thin film was directly used as a working electrode without any additive. The obtained mass was approximately 1 mg per membrane electrode. The counter electrode used was a lithium ribbon, and the separator was Celgard 2300. Moreover, a 1 M LiPF$_6$ dissolved in 1/1 (V/V) ethylene carbonate/ethylmethyl carbonate was used as the electrolyte. Cyclic voltammetry (CV) and electrochemical impedance spectroscopy (EIS) were performed by an electrochemical workstation (PARSTAT 2273) with a scan rate of 0.1 mV/s from 0.00 to 3.00 V. Charge (lithium insertion) and discharge (lithium extraction) tests were performed in a multi-channel battery test system (NEWARE, Shenzhen, China) at different rates from cut-off potential 0.01 V to 3.00 V.

3. RESULTS AND DISCUSSION

The schematic of the porous carbon nanofibers material design is shown in Fig. 1. First, the PVP/NaCl polymer nanofiber thin film was obtained by electrospinning homogeneous viscous solutions with NaCl dissolved in PVP. The obtained polymer thin film was stabilized (280 °C) for 2 h and then carbonized (600 °C) for 2 h. During the stabilization process, PVP underwent cyclization and

cross-linking reactions, which resulted in a more stable nanofiber structure. Therefore, after carbonization, the polymer thin film changed into C/NaCl thin film with the fiber structure. Finally, by rinsing the C/NaCl nanofiber thin film with deionized water, NaCl was dissolved, which rendered the nanofiber change from solid to porous. We obtained the porous carbon nanofiber thin film. The as-prepared porous carbon nanofiber film can be bent, exhibiting good flexibility. A large number of mesopores were distributed in each nanofiber.
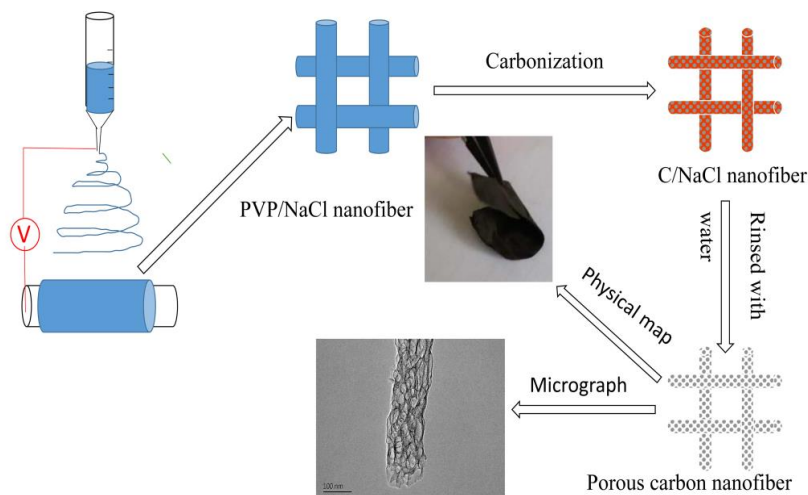

Figure 1. Schematic of the material design of porous carbon nanofibers.
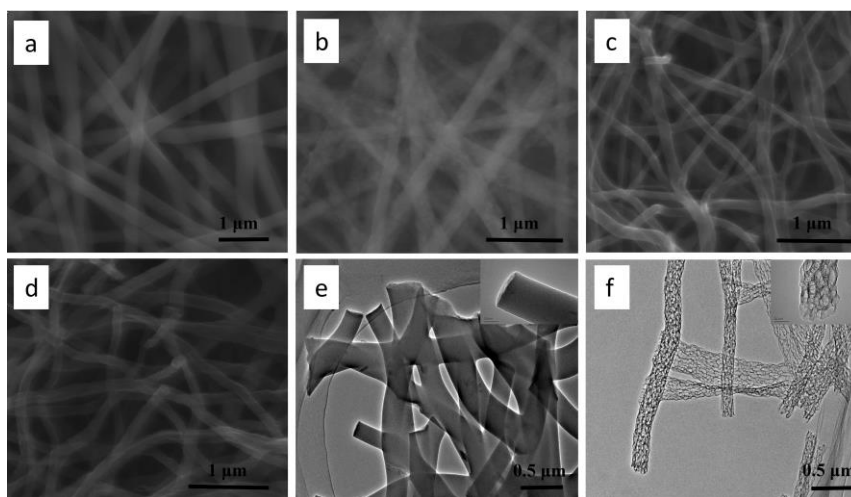

Figure 2. SEM micrographs of electrospun fibers; (a) PVP nanofibers; (b) PVP/NaCl nanofibers; (c) carbonized PVP nanofibers; (d) porous carbon nanofibers (water-rinsed carbonized PVP/NaCl nanofibers). TEM image and pore structure of the fibers, (e) carbon nanofibers; (f) porous carbon nanofibers.

To study the microstructure of the material, we observed the microstructure of all fibers using SEM and TEM. The SEM and TEM images of the as-prepared flexible nanofiber thin films including porous carbon nanofiber film (water-rinsed carbonized PVP/NaCl nanofibers) and its contrast samples (PVP nanofiber film; PVP/NaCl nanofiber film and carbonized PVP nanofiber film) are shown in Fig. 2. All electrospun fibers are straight and exhibit an interconnected structure, uniformly distributed

diameters, and irregular net structure without beads. The diameter of the PVP fibers is 300–400 nm (Fig. 2a). The diameter of the PVP/NaCl fibers shown in Fig. 2b is 200–300 nm, along with some small NaCl particles evenly distributed on the fiber surface. This characteristic of fiber diameters for PVP/NaCl fibers was caused by the increased precursor viscosity after the addition of NaCl. To improve the electrical conductivity of the composite films, we performed a simple carbonization treatment. After carbonization, the diameter of the fibers decreased to 200–300 and 150–200 nm for pure PVP- and PVP/NaCl-derived carbon fibers, respectively. The shrinkage of all fibers was mainly caused by the release of gases (CO_2, CO, and H_2O). The carbon nanofibers still exhibited uniform cylindrical fibers (Fig. 2c); however, the carbonization PVP/NaCl nanofibers exhibited rugged anomalistic cylindrical fibers (Fig. 3). These obvious differences are attributed to the formation of NaCl crystal particles at a high temperature. Interestingly, the porous carbon nanofibers with highly porous structure were easily and rapidly obtained after rinsing the carbonization PVP/NaCl nanofibers with deionized water. As shown in Fig. 2d, numerous folds were observed on the fiber surface; the fiber diameter is uniform due to the uniform distribution of NaCl in the fiber and the uniform particle size of NaCl. The highly porous structure was also observed in the TEM image of the porous carbon nanofiber thin film samples in Fig. 2f and the carbonized PVP fiber thin film (Fig. 2e) samples in the control experiment. Numerous honeycomb-like pores were rapidly formed and evenly distributed in the nanofiber owing to the rapid dissolution of NaCl crystal particles.
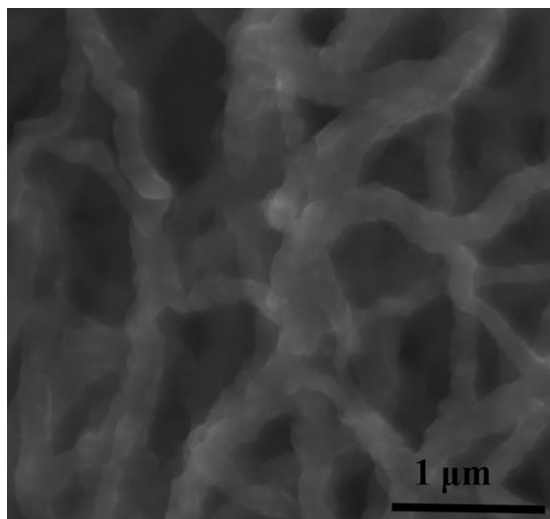

Figure 3. SEM micrographs of C/NaCl nanofibers

In this fabrication process for the flexible porous carbon nanofiber thin film, the addition of NaCl is expected to play three important roles: 1) During electrospinning, the addition of NaCl changes the precursor viscosity resulting in the slim fiber; 2) During carbonization, the change of NaCl crystal at a high temperature helps in the formation of several folds on the surface of the fibers; 3) During rinsing, NaCl as a pore-forming agent rapidly dissolves in water, resulting in the formation and even distribution of honeycomb-like pores in the flexible nanofiber film samples.
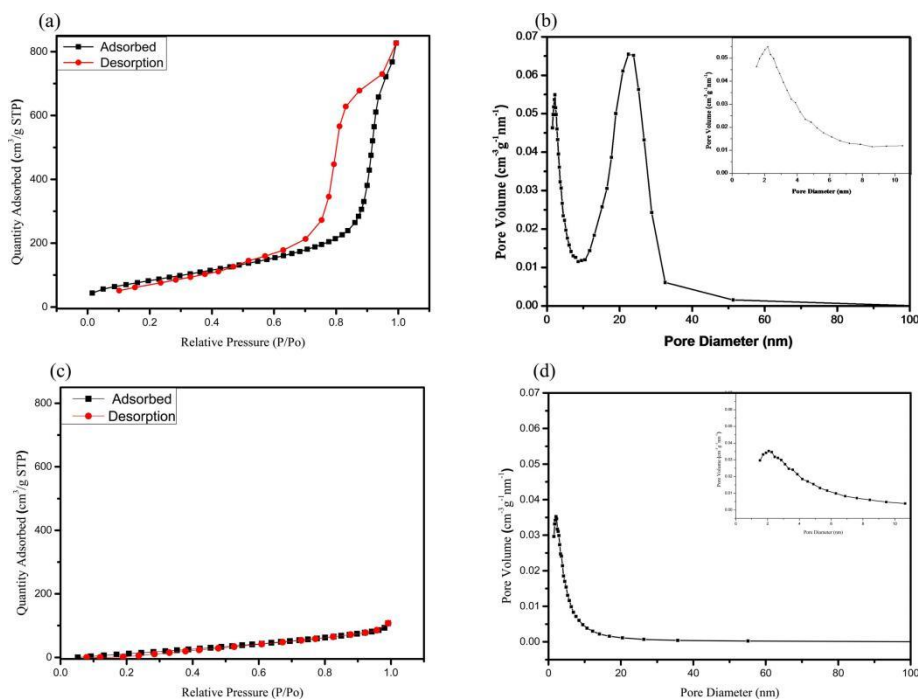
Figure 4. (a) N_2 adsorption–desorption isotherms of porous carbon fibers; (b) pore size distribution of porous carbon fibers. (c) N_2 adsorption–desorption isotherms of carbon fibers; (d) pore-size distributions of carbon fibers;

The surface area and size distribution are important factors in improving the wettability between electrode materials and electrolyte. To obtain such information about the porous carbon nanofiber thin film, researchers studied the N_2 adsorption/desorption isotherms and measured the derived pore size distribution curve using the Barrett–Joyner–Halenda method for the thin film specimen of porous carbon nanofibers (Fig. 4). Typically, the N_2 adsorption–desorption isotherm shows a model IV isotherm with H3-type hysteresis loop. The hysteretic loop between the adsorption and desorption curves with a low relative pressure (<0.4) are contributed by micropores, indicating the existence of mesopores under moderate relative pressure (0.4–0.8). In addition, the rapid increase in the N_2 uptakes at a high pressure (>0.90) indicates the presence of some macropores in the nanofibers. The specific surface area of the porous carbon nanofibers is 315.69 m^2/g, which is higher compared with that of the carbon nanofibers (138.96 m^2/g). Moreover, the pore-size distributions of the porous carbon fibers are mesopore and micropore (Fig. 4a,b), and the adsorption of the carbon nanofibers was contributed by micropores (Fig. 4c,d). These findings suggest that the micropores of the pure PVP-derived fibers were produced during heat treatment owing to the release of gases and that the removal of NaCl in the PVP/NaCl-derived fibers created large quantities of mesopores. The presence of the mesopores ensures the distribution of the electrolyte ions into the carbonaceous electrode [32,33]. However, because micropores are hard wetted by electrolytes, they are unfavorable for rapid ion distribution. Hence, the presence of large quantities of mesopores in fiber thin films is crucial to enhance the electrochemical performance of carbon nanofibers. Interestingly, the specific surface area of the fiber thin films obviously increased with the addition of NaCl. This finding is understandable because PVP/NaCl-derived carbon fibers possess finer fiber diameters and larger pore volumes

compared with pure PVP-derived carbon fibers. When used as an anode for LIBs, the highly porous surface structure increased the surface area of the material and significantly increased the lithium ion storage sites. This particularly porous network structure furnished a shortened lithium ion transmission distance and a wide-ranging interface between the electrolyte and the material. Thus, charge-transfer reaction speeds were accelerated.
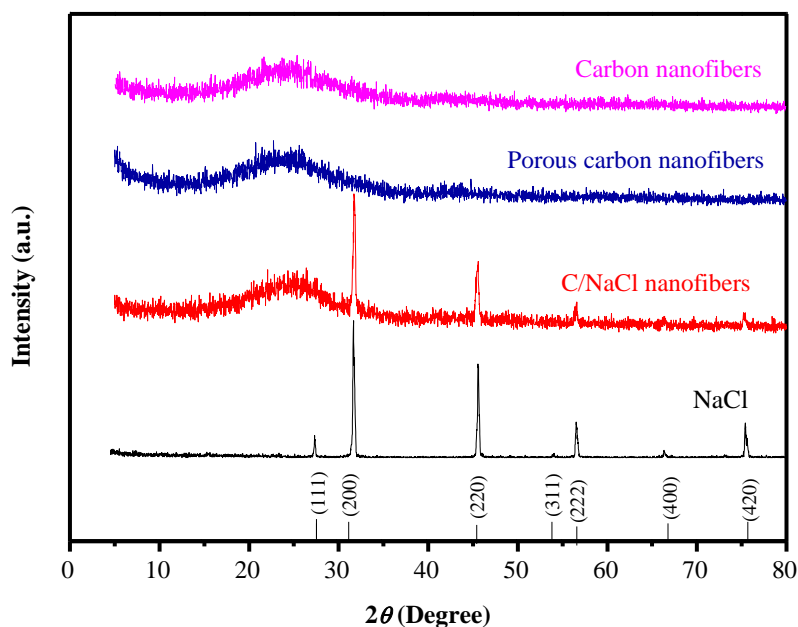

Figure 5. XRD pattern analysis of porous carbon nanofibers, carbon nanofibers, C/NaCl, NaCl, nanofibers,

Fig. 5 shows the XRD pattern of the porous carbon nanofibers, carbon nanofibers, C/NaCl nanofibers, and NaCl samples. The C/NaCl nanofibers exhibited diffraction peaks at $2\theta(°) = 27.37$, 31.7, 45.45, 53.87, 56.47, 66.23, and 73.07 corresponding to the (111), (200), (220), (311), (222), (400), and (420) planes, respectively, which all matched the characteristic diffraction peaks of NaCl. However, the carbon nanofibers and porous carbon fibers presents two broad repercussions. At 2θ of 25°, a sharp peak corresponded to the (002) graphitic layers; at 2θ of 45° an inferior peak showed the (100) disordered carbon flat [34]. These XRD patterns indicate that NaCl was completely removed after rinsing with deionized water and that the remaining material is pure carbon. Post-treatment of the material only requires a simple and fast washing process, and avoids treatment with acidic or basic solutions. Furthermore, the used NaCl can be recycled, which significantly reduces the preparation cost.
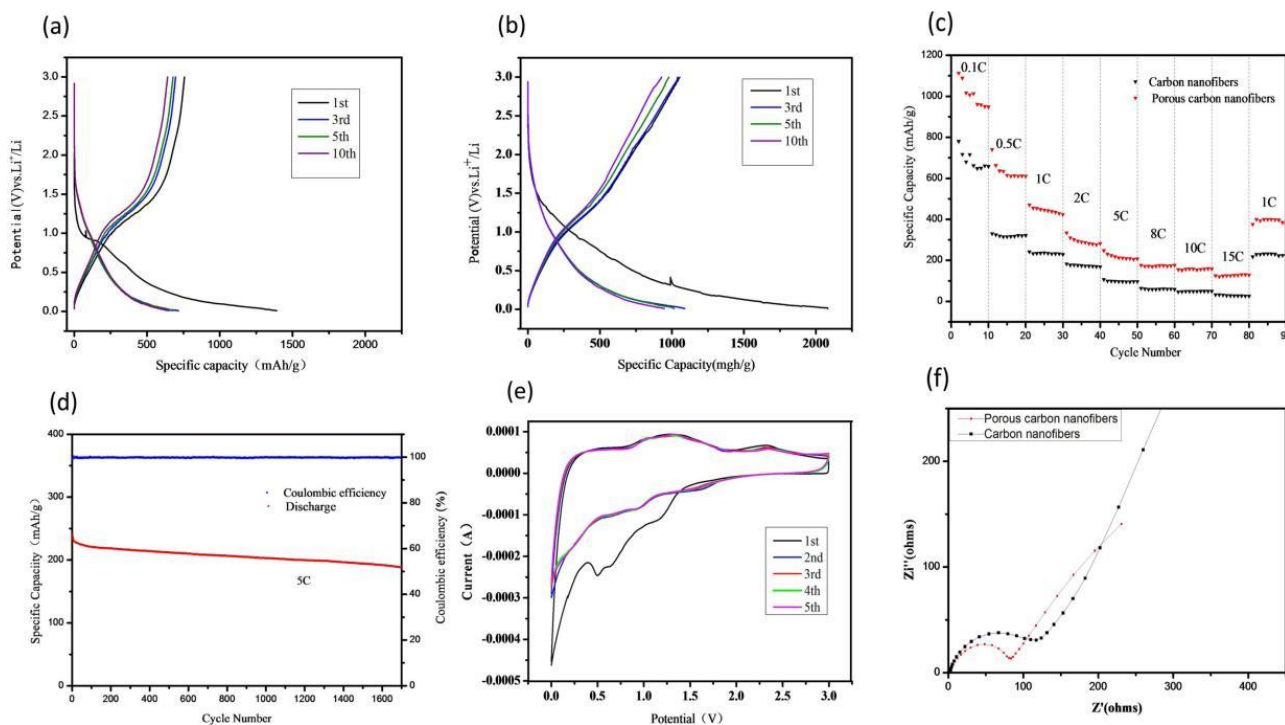
Figure 6. (a) Initial discharge–charge curves of the carbon nanofibers at 0.1C; (b) initial discharge–charge curves of porous carbon nanofibers at 0.1C; (c) rate performance of carbon nanofibers and porous carbon nanofibers; (d) long-term cycling performance and coulombic efficiency of porous carbon nanofibers at 5C; (e) CV curves of porous carbon nanofibers at 0.1 mV/s; (f) electrochemical impedance spectra of different materials.

The carbon nanofiber thin films were used directly as anodes for LIBs. The galvanostatic charge–discharge curves of the porous carbon nanofibers and the carbon nanofibers in the first 10 cycles at 0.1C are shown in Fig. 6(a,b). The cells showed that the first discharge capacities were at 2100 and 1400 mAh·g^{-1} for the porous carbon nanofibers and the carbon nanofibers, respectively. Furthermore, the following charged capacities were 1150 and 700 mAh·g^{-1} for the porous carbon nanofibers and the carbon nanofibers, respectively. The reversible capacities of the carbon nanofibers and the porous carbon nanofibers were approximately 50% and 57% at the first cycle, respectively. A 100% reversible capacity cannot be achieved due to the formation of the SEI layer [35] and the structural blemish depleting the extra lithium ions [36–38]. When the discharge–charge test was between the 3rd and 10th cycles, an improved discharge capacity of 1000 mAh·g^{-1} for the porous carbon fiber thin film was obtained, whereas a discharge capacity of only 680 mAh/g was demonstrated by the counterpart carbon fiber film. Moreover, almost all the discharge profiles showed the characteristic features of C, and the potentials of these composite film electrodes with the highest capacity were within 0.2–0.7 V. These results indicate that the composite materials are suitable for anodes.

To investigate the rate performance of the porous carbon nanofiber film sample, the rate capabilities of porous carbon nanofiber and carbon nanofiber samples as electrode materials were

tested at distinct C-rates (C) of 0.1, 0.5, 1, 2, 5, 8, 10, and 15 (Fig. 6c). The porous carbon nanofiber film displayed a higher capacity at all rates compared with the baseline sample of the carbon fiber film because of the large quantities of mesopores, surface folds, and high-specific surface area of the former. The porous carbon nanofiber film exhibited high specific capacities of 948.1, 610.7, 425.3, 301.6, 228.9, 193.5, 171.7, and 119.2 mAh/g (mean) at C-rates of 0.1C, 0.5C, 1.0C, 2.0C, 5.0C, 8C, 10C, and 15C, respectively. Moreover, when the current density was switched back to 1C after 80 cycles at different C-rates, the charge capacity of 420.9 mAh g^{-1} at 1C was recovered, allowing a high capacity retention of 99.0%. Interestingly, the reversible capacity of this novel film electrode of the porous carbon fiber thin film can reach 208.8 mAg^{-1} after 1700 cycles, and the coulombic efficiency can reach 83.5% (Fig. 6d) at 5C (1860 mA/g). To the best of our knowledge, this value is the best rate capacity ever reported for porous carbon fiber thin film-based LIBs (Table 1). The high capacity retention and rate capabilities are indicative of the favorable electrolyte contact and reversible lithiation and delithiation transformation in the porous carbon fiber thin film samples, thereby ensuring repeatability and reversibility in successive cycling processes.

Table 1. Electrochemical performance of carbon nanofiber anodes reported in previous studies and in this work

Products	First charge capacity (mAh g^{-1})	Current density (mA g^{-1})	Cycling performance Residual capacity (mAhg^{-1}) /current (mA g^{-1})/ cycle number	Reference
Carbon nanofibers	621	48.36	454 /48/50th cycle	[26]
Pore-structure-optimized CNT-carbon fibers	743	37.2	510 /37.2/30th cycle	[27]
Porous carbon nanofibers	446	150	354 /200/100th cycle	[28]
Porous carbon nanofibers	593	50	380 /50/10th cycle	[29]
N-doped carbon nanofibers with open-channels	734	74.4	330 /372/500th cycle	[30]
Carbon nanofibers	452	20	255 /200/200th cycle	[31]
Porous carbon nanofibers	1150	37.2	208.8/1860/1700thcycle	This work

To understand the kinetics of the porous carbon fiber thin film electrodes, we displayed the results of CV and EIS measurements in Fig. 6e and f, respectively. Fig. 6e shows the CV curves of the porous carbon nanofibers for the first five cycles in the potential window of 0–3.00 V. At the initial cycle of cathodic sweep, two peaks (lithium insertion) were observed at 0.5 and 1.1 V. These peaks

were attributed to the disintegration of electrolytes to form the SEI layer and irreversible lithium insertion reactions. However, these characteristics disappeared in the next cycles, indicating that the SEI layer was completely formed. After the first cycle, the subsequent CV patterns were almost similar, indicating the reversible lithiation and delithiation processes.

The EIS profiles of the cells with porous carbon nanofibers and carbon nanofibers thin film electrodes were collected and are presented in Fig. 6f. The Nyquist plot displays a depressed semicircle consisting of charge transfer resistance [39] and interfacial resistance [40]. The straight line is assigned to the diffusion and transport of the Li^+ from the electrolyte to the electrode surface. The resistance of the porous carbon nanofibers (80 Ω) is much lower than that of the carbon nanofibers (125 Ω), indicating that the special structure of the porous carbon nanofibers further promotes the electronic conductivity of composites. Moreover, the particularly porous network structure provides shortened pathways for Li^+ transport and offers an extensive interface with the electrolytes.

4. CONCLUSION

We fabricated a highly porous carbon nanofiber thin film as a high-performance LIB anode. The fabrication process comprised simple electrospinning and rapid water washing processes. The used NaCl can be recycled, thereby significantly reducing the preparation cost of the porous fiber thin film. Interestingly, the as-prepared nanofiber thin film displays a highly porous surface, an interconnected porous network, and significantly increased lithium ion storage sites. When used for LIBs anodes, it exhibited good electrochemical performance and could deliver a large capacity (948.1 mAh·g^{-1} at 0.1C), a long cycle life (at 5C charge capacity can reach 208.8 mAh·g^{-1} after 1700 cycles), and a high coulombic efficiency (more than 99%). This work illustrates a new low-cost method of preparing high-value porous carbon fiber thin film electrodes.

References

1. Barranco, V. Lillo-Rodenas, M. A. Linares-Solano, A. Oya, A. Pico, F. Ibanez, J. Agullo-Rueda, F. Amarilla, J. M. Rojo and J. M, J., *Phys. Chem. C.,* 114 (2010) 10302.
2. Kim, C. Yang and K. S, *Appl. Phys. Lett.,* 83 (2003) 1216.
3. Yoon, S. H. Park, C. W. Yang, H. J. Korai, Y. Mochida, I. Baker, R. T. K. Rodriguez and N. M., *Carbon,* 42 (2004) 21.
4. Mathur, R. B. Maheshwari, P. H. Dhami, T. L. Sharma, R. K. Sharma and C. P., *J. Power Sources,* 161 (2006) 790.
5. J. M. Tarascon and M. Armand, *Nature,* 414 (2001) 359.
6. P. Balaya, *Energy Environ. Sci.,* 1 (2008) 645.
7. A. Manthiram, A. V. Murugan, A. Sarkar and T. Muraliganth, *Energy Environ. Sci.,* 1 (2008) 621.

8. P. G. Bruce, B. Scrosati and J. M. Tarascon, *Angew. Chem. Int. Ed.,* 47 (2008) 2930.
9. F. Cheng, Z. Tao, J. Liang and J. Chen, *Mater.,* 20 (2008) 667.
10. Y. G. Guo, J. S. Hu and L. J. Wan, *Adv. Mater.,* 20 (2008) 2878.
11. M. G. Kim and J. Cho, *Adv. Funct. Mater.,* 19 (2009) 1497.
12. J. M. Tarascon and M. Armand, *Nature,* 414 (2001) 359.
13. Hu, Y. S. Adelhelm, P. Smarsly, B. M. Hore, S. Antonietti and M. Maier, J., *Adv. Funct. Mater.,* 17 (2007) 1873.
14. Kaskhedikar, N. A. Maier and J., *Adv. Mater.,* 21(2009) 2664.
15. E. Yoo, J. Kim, E. Hosono, H. S. Zhou, T. Kudo and I. Honma, *Nano Lett.,* 8 (2008) 2277.
16. S. Chen, P. Chen and Y. Wang, *Nanoscale,* 3 (2011) 4323.
17. L. Ren, K. N. Hui, K. S. Hui, Y. Liu, X. Qi, J. Zhong, Y. Du and J. Yang, *Sci. Rep.,* 5 (2015) 14229.
18. A. L. M. Reddy, A. Srivastava, S. R. Gowda, H. Gullapalli, M. Dubey and P. M. Ajayan, *ACS Nano.,* 4 (2010) 6337.
19. G. Wang, X. Shen, J. Yao and J. Park, *Carbon,* 47 (2009) 2049.
20. Z. J. Fan, J. Yan, T. Wei, G. Q. Ning, L. J. Zhi, J. C. Liu, D. X. Cao, G. L. Wang and F. Wei, *ACS Nano.,* 5 (2011) 2787.
21. R. W. Pekala, J. C. Farmer, C. T. Alviso, T. D. Tran, S. T. Mayer, J. M. Miller and B. Dunn, *J. Non-Cryst.,* 255 (1998) 74.
22. G. R. Sun, L.Q. Sun, H. M. Xie and J. Liu, *Nanomaterials,* 6 (2016) 129.
23. M. Inagaki, Y. Yang and F. Kang, *Adv. Mater.,* 24 (2012) 2547.
24. L. Dong, G. Wang, X. Li, D. Xiong, B. Yan, B. Chen, D. Li and Y. Cui, *RSC Adv.,* 6 (2016) 4193.
25. D. Nan, Z.-H. Huang, R. Lv, L. Yang, J.-G. Wang, W. Shen, Y. Lin, X. Yu, L. Ye, H. Sung and F. Kang, *J. Mater.Chem. A.,* 2 (2014) 19678.
26. L. W. Ji, Y. F. Yao, O. Toprakci, Z. Lin, Y.Z. Liang, Q. Shi, A. J. Medford, C. R. Millns, X.W. Zhang and L. Ji . *J.Power Sources,* 195 (2010) 2050.
27. Y.J. Jeong, K. Lee, K. Kim and S. Kim, *Materials,* 9 (2016) 995.
28. Y. T. Peng and C. T. Lo, *J Solid State Electrochem.,* 19 (2015) 3401.
29. L.W. Ji, Z. Lin, A. J. Medford and X. W. Zhang, *Carbon.,* 47 (2009) 3346.
30. S. W. Park, J. C. Kim, M. A. Dar, H. W. Shim and D. W. Kim, *Chem. Eng. J.,* 315 (2017) 1.
31. Shi, Z. Chong, C. Wang, J. Wang, C. Yu and X., *Mater. Lett.,* 159 (2015) 341.
32. X. K, Q. Gao, J. Jiang and J. Hu, *Carbon,* 46 (2008) 1718.
33. A. B. Fuertes, G. Lota, T. A. Centeno and E. Frackowiak, *Electrochim. Acta,* 50 (2005) 2799.
34. G. J. Lee and S. I. Pyun, *Electrochim. Acta,* 51 (2006) 3029.
35. C. Wang, A. J. Appleby and E. F.Little, *J Electroanal Chem.,* 519 (2002) 9.
36. P. S. Kumar, R. Sahay, V. Aravindan, J. Sundaramurthy, W. C. Ling, V. Thavasi, S. G. Mhaisalkar, S. Madhavi and S. Ramakrishna, *J Phys D: Appl Phys.,* 45 (2012) 265302.
37. V. Subramanian, H. Zhu and B. Wei, *J Phys Chem B.,* 110 (2006) 7178.
38. J. S. Kim and Y. T. Park, *J Power Sources,* 91 (2000) 172.
39. K. Xu, S. Zhang and R. Jow, *J. Power Sources,* 143 (2005) 197.
40. Y. Zhang, C. Y. Wang and X. Tang, *J. Power Sources,* 196 (2011) 1513.